Journal Name

ARTICLE TYPE

Cite this: DOI: 00.0000/xxxxxxxxxx

Computational discovery of high charge mobility self-assembling π -conjugated peptides †

Kirill Shmilovich, $^{\ddagger a}$ Yifan Yao, $^{\ddagger b}$, John D. Tovar c,d , Howard E. Katz d , André Schleife, *b and Andrew L. Ferguson *a

Received Date Accepted Date

DOI: 00.0000/xxxxxxxxxx

Organic electronics offer a route toward electronically active biocompatible soft materials capable of interfacing with biological and living systems. One class of promising organic electronic materials are π -conjugated peptides, synthetic molecules comprising an aromatic core flanked by oligopeptides, that can be engineered to self-assemble into elongated nanostructures with emergent optoelectronic functionality. In this work, we combine molecular dynamics simulations with electronic structure and charge transport calculations to computationally screen for high charge mobility π -conjugated peptides and to elucidate design rules linking aromatic core character with charge mobility. We consider within our screening library variations in the aromatic core chemistry and length of the alkyl chains connecting the oligopeptide wings to the core. After completing our computational screen we identify particular π -conjugated peptides capable of producing self-assembled biocompatible nanoaggregates with predicted hole mobilities of 0.224 cm²/(Vs) and electron mobilities of 0.143 cm²/(Vs), and uncover design rules that enhance understanding of the molecular determinants of charge mobility within π -conjugated peptide assemblies.

Design, System, Application

Synthetic π -conjugated peptides comprising an aromatic core flanked by oligopeptide wings can be engineered to self-assemble into elongated nanoaggregates with emergent optical and electronic functionality. These molecules present promising building blocks for the fabrication of biocompatible organic electronics. The molecular determinants governing the emergent self-assembled morphologies and electron and hole transport characteristics are not well understood, which has frustrated rational molecular design. In this work, we integrate classical molecular dynamics simulations, electronic structure calculations, and Marcus theory calculations to screen a library of candidate π -conjugated peptides comprising different π -cores and alkyl spacer lengths linking the cores and wings. Our computational screen identifies molecules that spontaneously assemble into biocompat-

ible nanoaggregates with high predicted charge mobilities and exposes design rules linking molecular properties to the emergent structure and charge mobility. These results offer new guidelines and candidates for future experimental synthesis and testing. Our screening approach is generically extensible to other self-assembling organic semiconductors.

1 Introduction

Organic semiconductors have demonstrated impressive performance in recent applications to bio-sensing 1 and in photovoltaics^{2,3}. Organic semiconductors maintain the advantage of being mechanically flexible, lightweight, and possessing inexpensive solution processability compared to traditional silicon-based semiconductors. One class of promising organic semiconductors are π -conjugated peptides composed of a central π -core flanked by oligopeptide wings representing biocompatible building blocks for the bottom-up construction of nanoaggregates with tunable optical and electronic properties 4-10. These peptide based assemblies form elongated and hierarchical nanostructures driven by a combination of hydrogen bonding, van der Waals interactions, and intermolecular π - π stacking ^{11–14}. Structural and optoelectronic characteristics of supramolecular π -conjugated assemblies are amenable to a variety of human controlled modulation such as salt concentration, temperature, pH, flow, and light $^{14-20}$. Materials built from π -conjugated peptides are capable of long-range charge transport within aqueous and biologically relevant environments that can enable device construction

 $^{^{\}ddagger}$ These authors contributed equally to this work

^a Pritzker School of Molecular Engineering, University of Chicago, Chicago, Illinois 60637, USA.

b Department of Materials Science and Engineering, University of Illinois, Urbana-Champaign, Urbana, Illinois 61801, USA.

^c Department of Chemistry, Johns Hopkins University, 3400 North Charles Street, Baltimore, Maryland 21218, USA.

^d Department of Materials Science and Engineering, Johns Hopkins University, 3400 North Charles Street, Baltimore, Maryland 21218, USA.

^{*} E-mail: schleife@illinois.edu, andrewferguson@uchicago.edu

 $[\]dagger$ Electronic Supplementary Information (ESI) available: See DOI: 00.0000/000000000.

of solar cells and field-effect transistors for a plethora of functional applications in photovoltaic energy harvesting and power generation $^{6,21-28}$. Although crystalline electronic devices tend to support higher charge mobilities, organic electronics such as π -conjugated peptides benefit from biocompatibility and conformational flexibility that make them ideally suited to interface with biological and living systems such as photosynthetic machinery for energy harvesting or engineering interfaces with living cells. An important design challenge is to maximize charge mobility within π -conjugated peptide-based materials by controlling the molecular chemistry of these molecules.

Interchanging the different molecular building blocks that make up π -conjugated peptides enables precise tunablity and customizability over their emergent optical and electronic properties. For example, our previous work explored the influence that the variation of individual amino acids within the peptide wing can have on the emergent supramolecular chirality and structure of self-assembled π -conjugated peptide nanoaggregates²⁹. The role of alkyl spacers on molecular properties has previously been explored in the context of alkyl chains connecting the peptide wings to the core in π -conjugated peptides 30,31 , as well as for other systems such as zwitterionic polymer brushes 32,33. We also studied the impact of varying the length of the oligothiophene aromatic cores upon self-assembled π -conjugated peptide morphologies as a function of ionic strength, pH, temperature, and peptide concentration 20. Computational work has employed all-atom and coarse-grained molecular dynamics simulations and electronic structure calculations to elucidate π conjugated peptide self-assembly kinetics, thermodynamics, and electronic properties 16,27,34,35. Other works have engaged families of π -conjugated peptides using simulations and/or machine learning to establish design rules linking components of their chemical character to self-assembly and molecular packing behavior 36-38. Recently, we developed an integrated computationalexperimental framework to propose, synthesize, and characterize high-performing π -conjugated peptides with desirable electronic properties containing a fixed quaterthiophene core within the vast combinatorial space of varying length and composition peptide wings³⁹. In this work, we build upon these foundations to explore the influence of π -core chemistry and the length of the alkyl spacer linking the core to the wings upon the self-assembled morphologies and emergent charge mobility within the resulting nanoaggregates.

A detailed understanding of the structure-(electronic) property relationships in π -conjugated peptides is a prerequisite toward systematic improvement and engineering of high charge mobility. Although theoretical developments in the transport properties of organic semiconductors and their dependence on intra- and inter-molecular morphology has proved challenging 40 , a number of promising methods have been proposed in recent years to better understand the relationship between molecular structure and charge transport 41,42 . For example, in Ref. 43 the authors perform high-throughput virtual screening of novel crystalline dinaphtho[2,3-b:2',3'-f]thieno[3,2-b]thiophene derivatives using Marcus theory 44,45 to discover organic crystals with high levels of theoretical hole mobility. Here, we apply these methods

for calculating charge mobility to π -conjugated peptides which are inherently disordered, biocompatible molecular systems. As π -conjugated peptide nanostructures lack a well-defined crystal structure, we employ molecular dynamics simulations to predict their molecular packing behavior and self-assembled morphologies. We then apply density functional theory to ascertain the capacity for charge mobility within these nanoaggregates. Chemical stability is assessed by comparing reduction/oxidation potential of the species to baseline water reduction/oxidation potentials to determine the p/n-type nature of each molecule, and charge mobility is quantified by adopting a Marcus hopping model⁴³ that predicts the transfer rate of holes/electrons between molecules. Combining density functional theory and molecular dynamics simulations in this way enables us to probe the electronic behavior of self-assembled π -conjugated peptide nanostructures and identify promising candidate molecules anticipated to display good charge mobility.

We employ our combined molecular dynamics simulations and density functional theory workflow to investigate charge transport properties within a library of π -conjugated peptides. In particular, we attempt to optimize both the aromatic chemistry among a number of synthetically available cores and the alkyl linker length between the aromatic core and the peptide wings of π -conjugated peptides (Fig. 1). These two molecular determinants are anticipated to affect both the structural arrangement and packing of the self-assembled nanoaggregate structures and the degree of electronic coupling between the cores and wings. Each π -conjugated peptide studied here is built with VEVAG peptide wings, which is a prototypical oligopeptide sequence commonly known to mediate self-assembly and promote intermolecular π -electron delocalization ^{21,30,46}. The oligopeptide wings are symmetric so that the molecule possesses two C-termini and the N-termini are covalently bonded to the π -core via an alkyl spacer. This arrangement enables pH control over assembly. At high pH the carboxyl groups at the C-termini and glutamic acid side chains are deprotonated leading to a formal (-4) charge on each molecule that prevents large-scale assembly by Coulombic repulsion. At low pH the molecules become charge neutral and selfassembly proceeds driven by hydrophobicity, hydrogen bonding, and π - π stacking ^{28,36,39}.

The fixed VEVAG peptide wing flanks one of six arocores - (i) phenyl-thiophene-phenyl (PTP), (ii) bis(tetrafluorophenyl)thiophene (BFT), (iii) quarterthiophene (QTP), (iv) naphthalene-diimide (NDI), (v) perylene diimide (PDI), and (vi) benzo dithiophene (BDT) - and is linked to the core by a variable length alkyl chain containing n=0, 1, 2, or 3 carbon atoms. The six aromatic cores were selected from a combination of cores commonly used within the π -conjugated peptide literature and standalone aromatic structures that are well-established as performant organic semiconductor materials 21,47-52. The range of lengths of the alkyl chains were selected based on the known negligible π -electron delocalization operative through saturated carbon chains which was anticipated to isolate and decouple the electronics of the central π -electron core from any electronic influence of the peptide carboxamide linkers. Each π -conjugated peptide is then constructed with

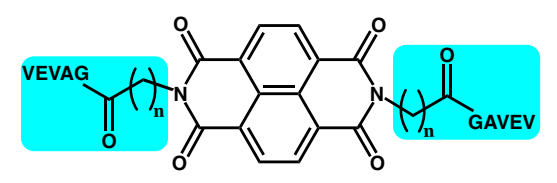
phenyl-thiophene-phenyl (PTP)

VEVAG S GAVE

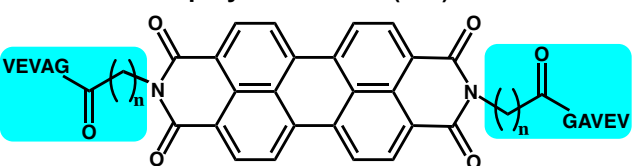
bis(tetrafluorophenyl)thiophene (BFT)

quaterthiophene (QTP)

naphthalene-diimide (NDI)



perylene diimide (PDI)



benzo dithiophene (BDT)

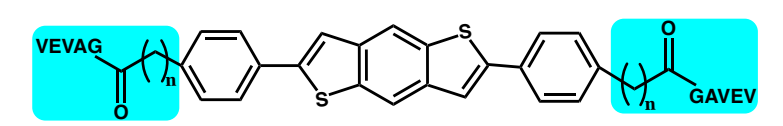


Fig. 1 Chemical structure of the different π -conjugated peptide molecules built from six unique aromatic cores that we screen in this work. The mirror symmetric oligopeptide wings VEVAG- Π -GAVEV are highlighted in blue and which flank one of six different aromatic cores $\Pi \in \{\text{PTP, BFT, QTP, NDI, PDI, BDT}\}$ separated from the wings by alkyl spacers of length $n \in \{0,1,2,3\}$. By considering all combinations of π -cores and alkyl chain lengths, our screening library comprises a total of $6 \times 4 = 24$ candidate π -conjugated peptide molecules.

VEVAG oligopeptides affixed to a π -core and separated from the peptide wing on each end with an alkyl spacer. By considering all combinations of π -cores and alkyl chain lengths, our library comprises a total of $6\times 4=24$ candidate π -conjugated peptide molecules (Fig. 1). Throughout this work we abbreviate the collection of molecules with a fixed aromatic core and varying spacer length as 'Lib-X', where X is the three-letter abbreviation corresponding to each aromatic core (e.g., Lib-PTP corresponds to π -conjugated peptides with a fixed phenyl-thiophene-phenyl core and the set of all $n \in \{0,1,2,3\}$ spacer lengths).

2 Methods

2.1 Overview of the computational pipeline

We establish a computational pipeline combining classical molecular dynamics (MD) simulations with density functional theory (DFT) electronic structure and Marcus theory charge mobility predictions to computationally screen π -conjugated peptides and discover candidate molecules predicted to self-assemble into nanoaggregates with high charge mobility. Unlike crystalline semiconductors with a well-defined crystal structure that can be directly probed with electronic structure calculations, π -conjugated peptide require us to first predict their molecular packing behavior and emergent nanoaggregate morphologies using MD simulations. We then perform DFT calculations to assess the stability and mobility of holes and electrons within these nanoaggregates. The predicted charge mobilities are a function of both the self-assembled morphology and the inherent electronic

properties of each candidate molecule. Our integrated MD/DFT screen can be represented schematically by the five-step protocol in Fig. 2, in which we (i) perform MD simulations of the assembly in water, (ii) determine hole/electron stability, (iii) calculate reorganization energy, (iv) calculate the transfer integral, and (v) combine the reorganization energy and transfer integral calculations to compute the intermolecular charge mobility from Marcus theory.

2.2 MD calculations

The GROMACS 2019.2 simulation suite was used to perform all molecular dynamics simulations 55. The Restrained Electrostatic Potential (RESP) method^{56,57} was used to derive partial charges for each molecule where calculations were performed at the B3LYP/6-31G(d) level of theory using the Gaussian 16 quantum chemistry software 58. All-atom topologies for each molecule were then generated using the AnteChamber PYthon Parser interfaceE (ACPYPE)⁵⁹ wrapper for ANTECHAM-BER (AmberTools17.0)60 and modeled with the AMBER99SB-IDLN⁶¹ forcefield. Each molecule was prepared in a charge neutral state with fully protonated glutamic acid residues corresponding to the low-pH conditions under which acid-triggered self-assembly proceeds ²⁸. Newton's equations of motion were solved and integrated forward with the leapfrog algorithm using a 2 fs timestep 62. Covalent bonds involving hydrogen atoms were constrained using the LINCS algorithm ⁶³. Lennard-Jones interactions were shifted smoothly to zero at a distance of 1.0

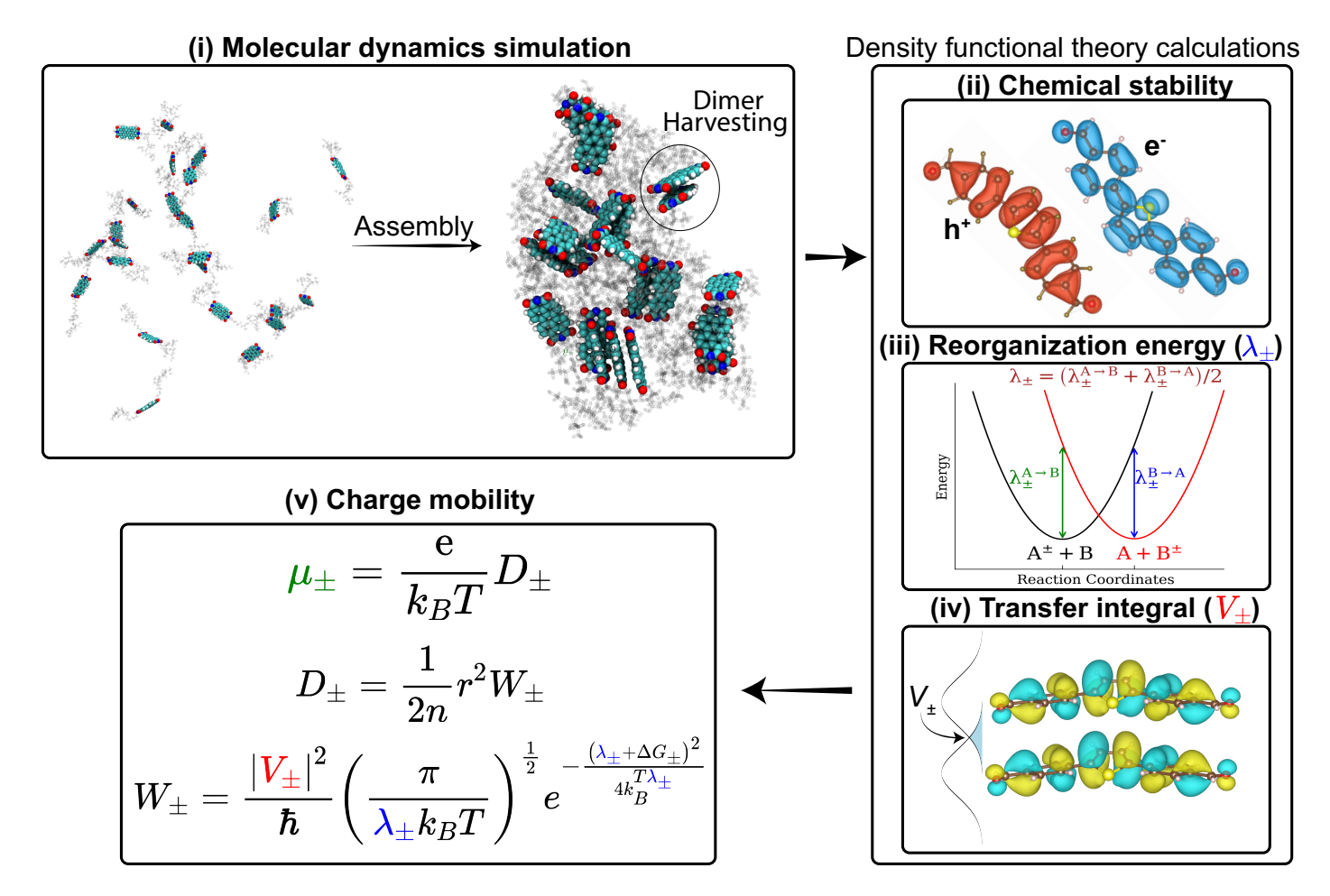


Fig. 2 Schematic illustration of our computational pipeline for measuring π -conjugated peptide charge mobility. (i) All-atom classical molecular dynamics (MD) simulations are conducted to predict the morphology of the self-assembled aggregates formed by each π -conjugated peptide. Electronically interacting dimer pairs are harvested and passed to density functional theory (DFT) calculations. DFT calculations are performed to compute (ii) the chemical stability of molecules supporting a hole or electron within an aqueous environment, (iii) the reorganization energy λ_{\pm} , and (iv) the transfer integral V_{\pm} . (v) Marcus theory is then used to predict the intermolecular drift mobility μ_{\pm} of holes/electrons within the nanoaggregates as a figure of merit for the potential optoelectronic functionality of the candidate π -conjugated peptide. Molecular visualizations were constructed using Visual Molecular Dynamics (VMD) ⁵³ and molecular orbitals visualized using VESTA ⁵⁴.

nm. Coulombic interactions were treated using particle mesh Ewald (PME) with a 1.0 nm real space cutoff and 0.16 nm Fourier grid spacing, and these values optimized for performance during runtime⁶⁴. Each system was initialized by placing 24 identical molecules randomly throughout a 12 x 12 x 12 nm³ simulation box with three-dimensional periodic boundary conditions, and subsequently solvating them with TIP3P water⁶⁵. Steepest descent energy minimization was then performed until forces larger than 1000 kJ/mol·nm were removed. Initial velocities were then sampled from a Maxwell-Boltzmann distribution at 300 K to perform an NVT equilibration at 300 K for 100 ps and subsequently an NPT equilibration at 300 K and 1 bar for 100 ps. Production runs were performed in the NPT ensemble for 500 ns at 300 K and 1 bar, where temperature was controlled using the velocity rescaling thermostat 66 and pressure controlled using the Parrinello-Rahman barostat⁶⁷. All simulations were performed on a single NVIDIA RTX 2080 Ti GPU achieving execution speeds of ~90 ns/day. These molecular dynamics simulation are carried out for all $4\times6=24$ molecules in our molecular design library. Input files and simulation trajectories for our MD calculations are provided as detailed in the Data Availability statement.

Over the course of the MD simulations, the initially monodisperse monomers self-assemble into nanoaggregates driven by van der Waals interactions, hydrogen bonding, and π - π stacking ^{36,39}. Nanoaggregate snapshots of Lib-PDI spacer 2 are visualized in Fig. 2, with the terminal self-assembled nanoaggregates for each π -conjugated peptide simulated in this work shown in Fig. S1a in the ESI[†]. To predict the charge transport properties within these nanoaggregates, we consider nearest neighbor interactions between dimers within the multimeric assembly, a method that is commonly employed in predicting the transport properties in organic crystals and amorphous organic materials 42. Rather than exhaustively considering all nearest neighbors as molecular dimers we focus our sampling to pairs of molecules most likely to interact electronically. Prior x-ray scattering and energy minimization calculations show that associated π -conjugated peptide molecules lie within a center of mass (COM) separation of $\sim 0.46 - 0.47$ nm^{68,69}. Based on this observation, we consider a pair of molecules to be an electronically interacting dimer within a given simulation snapshot if the COM distance $d_{i,j}$ between neighboring aromatic cores of molecules i and j satisfies $d_{i,j} \leq 0.5$ nm. We have previously reported that the total number of dimers serves as a suitable metric to evaluate convergence of the structural evolution of the π -conjugated peptide self-assembled nanoaggregates 36,39 . The total number of dimers meeting the $d_{i,j} \leq 0.5$ nm criterion to approximately stabilize after 375 ns (Fig. S1b in the ESI †), motivating us to extract dimers from frames harvested every 100 ps within the final 125 ns of each 500 ns simulation. We randomly select 50 dimer configurations to pass forward to the DFT calculations as a sufficiently large ensemble to gather reliable statistics while balancing the high computational cost of DFT simulations.

2.3 DFT calculations

As an initial preprocessing step for the dimer configurations extracted from the molecular dynamics simulations, the oligopeptide wings are removed from the π -conjugated peptide geometries and the electronic structure calculations are performed only on aromatic cores that include the alkyl spacer capped on each end with terminal aldehyde groups. The reasoning for this preprocessing step is two-fold. First, the various candidate molecules differ from one another in the identity of the π -core and the length of the alkyl spacer, however the identity of the oligopeptide wings is held constant for all candidates. The primary source of optoelectronic functionality in self-assembled π -conjugated peptide nanostructures stems from π -electron delocalization fostering charge transfer between neighboring aromatic cores ^{34,43,70}. The oligopeptide wings implicitly affect the charge mobility by mediating the relative intermolecular packing between molecules in the self-assembled nanoaggregates, but are understood to be quite electronically insulated from π -cores, particularly for long alkyl spacer lengths ³⁰. Secondly, the oligopeptide wings comprise a large number of atoms and therefore incur considerable expense within the electronic structure calculations. Assuming that intermolecular charge transfer is mainly governed by the π -cores, we truncate our dimer structures to only possess these most relevant components for charge mobility and enable a larger number of representative dimer configurations to be considered within our ensemble by greatly alleviating the computational expense of each single calculation.

We perform DFT calculations of the chemical stability, reorganization energy, and transfer integral. All calculations are performed on 50 dimer configurations extracted from MD simulations from which we estimate the mean and variability of the these quantities within the structural ensemble. For the transfer integral calculations, the orbital coefficients, orbital energies, and overlap matrices are calculated using DFT following the scheme described in Sec. 2.5.2. For the reorganization energy and chemical stability calculations, the geometries of each π -conjugated peptide monomer are relaxed separately from one another in the gas phase with single point energy calculations independently performed on each monomer. Solvation effects are additionally included for the chemical stability calculations by incorporating

the polarizable continuum model (PCM) 71 where water is used as the solvent. All DFT calculations employ the B3LYP 72,73 hybrid functional and the 6-311+G(D,P) basis set and are performed using the Gaussian 16 quantum chemistry code 58 . Input files and post-processing scripts for our DFT calculations and tabulated results of our chemical stability, reorganization energy, transfer integral, and charge mobility calculations are provided as detailed in the Data Availability statement.

2.4 Chemical Stability

The electrochemical reaction between water and a charged state polymer is a primary charge trapping and degradation pathway 74,75 . The chemical stability of the n-type organic semiconductor can be determined by evaluating the difference between the oxidation potential of the polymer anion and the reduction potential for the half reaction involving oxygen. Similarly, the chemical stability of the p-type semiconductor can be determined by the difference between the reduction potential of the polymer cation and the oxidation potential for the half reaction involving water 74 . Assuming a Standard Hydrogen Electrode (SHE) potential, the oxidation electrode potential of water is +1.23 V (SHE),

$$O_2 + 4H^+ + 4e^- \rightarrow 2H_2O,$$
 (1)

and the reduction electrode potential is -0.83 V (SHE) 76 ,

$$2H_2O + 2e^- \rightarrow H_2 + 2OH^-.$$
 (2)

For each monomer A within a dimer configuration the oxidation (+)/reduction (-) potential is given by,

$$\pm (E_{\pm}(A^{\pm}) - E_0(A^0)),$$
 (3)

where E_+ , E_- , and E_0 denote the total energy calculated in one of the cationic (+), anionic (-), or neutral (0) states, respectively. These total energies are computed for a monomer geometry given by the argument $E(\cdot)$ relaxed in either the cationic A^+ , anionic A^- , or neutral A^0 charge state. We screen for candidate molecules likely to have a stable cationic state with an ionization potential smaller than +1.23 V (SHE), and a stable anionic state with an electron affinity greater than -0.83 V (SHE). Molecule libraries which meet this criterion for a majority of spacer lengths are subsequently passed to further computational screening of their charge transport properties to identify candidates with the most potential as functional organic semiconductors. By conducting this chemical stability screen, we assure that only molecules capable of stably supporting holes or electrons within an aqueous environment are passed on to the charge mobility calculations.

2.5 Charge Mobility

The predicted charge mobility within the self-assembled nanoaggregate is a function of both the morphology of the aggregate and the intrinsic chemical properties of the constituent π -conjugated peptide monomers, and serves as the figure of merit by which to rank the performance of each candidate molecule. To measure charge mobility we adopt the hopping model described by Marcus theory ^{44,45}. We aim to maximize the drift mobility of holes

 μ_+ and electrons μ_- in molecular dimers given by the Einstein relation,

$$\mu_{\pm} = \frac{\mathrm{e}}{k_B T} D_{\pm},\tag{4}$$

where e is the electron charge. D_{\pm} is the hopping rate of holes/electrons and can be modeled under the dimer approximation as,

$$D_{\pm} = \frac{1}{2n} r^2 W_{\pm},\tag{5}$$

where n=3 is the spatial dimension, r is the COM distance between two neighboring molecules, and W_{\pm} is given by,

$$W_{\pm} = \frac{|V_{\pm}|^2}{\hbar} \left(\frac{\pi}{\lambda_{\pm} k_B T}\right)^{\frac{1}{2}} e^{-\frac{(\lambda_{\pm} + \Delta G_{\pm})^2}{4k_B T \lambda_{\pm}}},\tag{6}$$

where V_{\pm} is the transfer integral, λ_{\pm} is the reorganization energy, k_B is the Boltzmann constant, \hbar is the Planck constant, ΔG_{\pm} is the change of Gibbs free energy of the charge exchange process, and $T\!=\!300$ K is the temperature. In the following sections we present a detailed explication of how the reorganization energy and transfer integral terms are calculated.

2.5.1 Reorganization Energy

The reorganization energy λ_\pm measures the change in the free energy of the reactant state to its equilibrium configuration, which describes the energy required to relax the molecular geometry upon charge transfer. Smaller values for the reorganization energy imply less energetic hindrance upon charge transfer and result in higher charge mobility (Eqns. 4-6). Given a molecular dimer configuration, the reorganization energy $\lambda_\pm^{A\to B}$ for the charge transfer process $A^\pm + B \to A + B^\pm$ from, arbitrarily labeled, monomer A to monomer B, is given by a four-point energy calculation scheme 77,78 ,

$$\lambda_{+}^{A \to B} = E_{\pm}(B^{0}) - E_{\pm}(B^{\pm}) + E_{0}(A^{\pm}) - E_{0}(A^{0}),$$
 (7)

where each term is a single point energy calculation performed in the ionic state given by the subscript, one of cationic E_+ , anionic E_- , or neutral E_0 , and in the configuration determined by a geometry optimization that is performed in either the cationic \mathbf{A}^+ , anionic \mathbf{A}^- , or neutral \mathbf{A}^0 charge state given in the argument $E(\cdot)$. Calculating the reorganization energy for a molecular dimer is complicated by the fact that our configurations are taken from molecular dynamics simulation snapshots where the two monomers will be in different geometries, and therefore $\lambda_{\pm}^{\mathbf{A}\to\mathbf{B}}\neq\lambda_{\pm}^{\mathbf{B}\to\mathbf{A}}$. We estimate the reorganization energy as the average of these two charge transfer processes 77,79 ,

$$\lambda_{\pm} = \frac{(\lambda_{\pm}^{A \to B} + \lambda_{\pm}^{B \to A})}{2}, \tag{8}$$

where $\lambda_{\pm}^{A\to B}$ and $\lambda_{\pm}^{B\to A}$ are given in Eqn. 7. By performing this average in Eqn. 8 the reorganization energy λ_{\pm} for a dimer configuration remains permutationally invariant and implicitly considers both possible charge transfer processes.

2.5.2 Transfer Integral

The transfer integral V_{\pm} can be understood as characterizing the strength of electronic coupling between the two π -conjugated

peptide monomer orbitals. Larger values of the transfer integral imply more electronic overlap between neighboring π conjugated peptide molecules and result in higher charge mobility (Eqns. 4-6). Under the assumption that only the frontier orbital of each monomer interacts, the transfer integral is defined as $V_{\pm} = \langle \phi_A | H | \phi_B \rangle$, where ϕ_A and ϕ_B represent the frontier orbital of (arbitrarily labeled) monomer A or B, and H is the Kohn-Sham Hamiltonian. We compute transfer integrals following the protocol reported in Ref. 80 and illustrated schematically in Fig. S2 in the ESI[†]. Under the approximation that only the frontier orbitals will interact, for hole transport, ϕ_A and ϕ_B are given by the HOMO orbitals, while for electron transport they are given by the LUMO orbitals. The matrix elements of the Kohn-Sham Hamiltonian $H_{AB} = \langle \phi_A | H | \phi_B \rangle$ and the overlap matrix $S_{AB} = \langle \phi_A | \phi_B \rangle$ are calculated in the basis of the frontier orbitals of each monomer. Due to the non-orthonormality of the monomer frontier orbitals, the computed matrix element H_{AB} is then transformed into an orthonormalized basis by performing the Löwdin transformation, $\hat{H}_{AB} = S_{AB}^{-\frac{1}{2}} H_{AB} S_{AB}^{-\frac{1}{2}}$. The value for the transfer integral V_{\pm} is then given by the off-diagonal terms of \hat{H}_{AB} . We verify that the transfer integrals computed for isolated dimers are in good agreement with significantly more expensive calculations for the same dimer embedded within larger tetramer stacks (Fig. S3, Table S1 in the ESI[†]). This demonstrates that transfer integrals computed at the dimer level are good approximations for those within self-assembled nanoaggregates comprised of multiple associated molecules.

2.5.3 Approximating $\Delta G_+ = 0$

The change in Gibbs free energy $\Delta G_{\pm}^{A \to B}$ for a molecular dimer configuration measures the energetic gain or loss upon charge transfer from (arbitrarily labeled) monomer A to monomer B. This free energy difference is given by ⁷⁹,

$$\Delta G_{\pm}^{{\rm A} \to {\rm B}} = G_{\pm}({\rm B}^{\pm}) + G_0({\rm A}^0) - \left(G_{\pm}({\rm A}^{\pm}) + G_0({\rm B}^0)\right), \eqno(9)$$

where each term calculates the Gibbs free energy in the ionic state given in the subscript for monomer configurations obtained from performing geometry optimization in the charge state provided in the argument $G_+(\cdot)$. We note that explicitly calculating ΔG_{\pm} in Eqn. 9 is nontrivial due to entropic contributions in the Gibbs free energy at finite temperatures. Practitioners applying Marcus theory to calculate charge transfer of organic semiconductors have commonly taken $\Delta G_{\pm}=0$ when the individual monomers have well-defined crystal structures ⁴³. In crystalline systems the two charge carrying species A and B will have identical geometries resulting in the change in the Gibbs free to be precisely zero independent of the direction of the charge transfer process $\Delta G_{+}^{A\to B} = \Delta G_{+}^{B\to A} = 0$. The self-assembled π -conjugated nanoaggregates lack a well-defined crystal structure such that the two monomers in each electronically interacting dimer pair have slightly different geometries. This symmetry breaking will, in principle, result in nonzero ΔG_{\pm} for any single configuration, but it is expected that $\Delta G_{\pm} \rightarrow 0$ when averaged over a sufficiently large ensemble. In Fig. S4 in the ESI[†], we test this assumption by calculating the total energy difference $\Delta E = E_0(A^0) - E_0(B^0)$

within dimer pairs of the Lib-PTP system. We confirm that the average value for ΔE calculated over a progressively larger ensembles approaches zero $\Delta E \to 0$, as is expected by the indistinguishability of the two arbitrarily labeled monomers A and B. We adopt ΔE as a proxy for ΔG_{\pm} as the latter is computationally prohibitively expensive to calculate for large ensembles, but the observation of $\Delta E \to 0$ implies by indistinguishability arguments that $\Delta G_{\pm} \to 0$. As a result, although we appreciate that $\Delta G_{\pm} \neq 0$ for any individual configuration, the computational challenges in the finite temperature entropy calculation lead us to follow Ref. ⁴³ and make the simplifying assumption that $\Delta G_{\pm} = 0$ that is valid in the limit of sufficiently large dimer ensembles.

3 Results and Discussion

We now present the results of our MD and DFT calculations and their integration with Marcus theory to predict charge mobilities. We first present the results of our chemical stability calculations to identify stable cationic/anionic species (Fig. 3). The reorganization energy (Fig. 4) and transfer integral (Fig. 5) calculations are then combined using Eqns. 4-6 to calculate the predicted charge mobility (Fig. 6).

3.1 Chemical Stability

A prerequisite to charge mobility within our molecular nanoaggregates in aqueous environments is their ability to stably support electronically charged states in water to prevent charge trapping and degradation via electrochemical reactions with water molecules 74,75. By reference to the electrochemical water half reactions 74 and assuming a Standard Hydrogen Electrode (SHE) potential 76 , the oxidation potential of water is +1.23 V and the reduction potential is -0.83 V. Oligopeptides with ionization potentials smaller than +1.23 V (SHE) are capable of stably supporting the cationic state and can potentially serve as p-type organic semiconductor; those with electron affinities greater than -0.83V (SHE) are capable of stably supporting the anionic state and can potentially serve as n-type semiconductors. We report in Fig. 3a the ionization potential of each candidate molecule in our five libraries relative to the reduction potential of water, and in Fig. 3b their electron affinities relative to the oxidation potential of water.

We observe from Fig. 3a that, with the exception of the Lib-PTP spacer 0 molecule, molecules with all spacer lengths within the Lib-PTP, Lib-QTP, and Lib-BDT libraries display stable cationic states indicating that they are potential candidates as p-type semiconductors. The remaining libraries, Lib-BFT, Lib-NDI, and Lib-PDI are not predicted to support electrochemically stable cations and we do not consider them further as potential p-type semiconductors. We observe from Fig. 3b that all molecules within the Lib-NDI and Lib-PDI libraries have stable anionic states indicating that they are potential candidates for n-type semiconductors. With the exception of the Lib-BFT spacer 0 molecule that supports a marginally stable anion, none of the molecules in the Lib-PTP, Lib-BFT, Lib-QTP, and Lib-BDT libraries are predicted to support stable anionic states and are dropped from further consideration as potential n-type semiconductors. A recent review

in Ref. 81 highlights NDI derivatives and PDI derivatives as stable n-type semiconductors, which is consistent with our predictions. Only Lib-BFT was predicted to support neither stable cationic not stable anionic states in water. This finding is consistent with previous work showing that both hole and electron injection into this pi system are likely to be unfavorable by more than ~ 1 V relative to standard calomel or silver chloride reference electrodes, suggesting that neither holes nor electrons would be particularly stable 51 .

3.2 Reorganization Energy

Having completed an initial screen for chemical stability, we proceed to interrogate the charge mobility of the candidate aromatic cores displaying stability in water solvent beginning by calculating the reorganization energy. The reorganization energy describes the energetic gain that results from the distortion of the equilibrium geometry between neutral state and charged state. A small reorganization energy suggests the capability of fast photoinduced charge transfer and is desirable for high charge mobility (c.f., Eqn. 6). We present the DFT-calculated reorganization energies for holes and electrons in all chemically stable species within Fig. 4. We note that the reorganization energy associated with hole transport is smallest for Lib-BDT (Fig. 4a), whereas that associated with electron transport is smallest for Lib-PDI (Fig. 4b). As a point of comparison, the reorganization energy of dinaphtho[2,3-b:2',3'-f]thieno[3,2-b]thiophene (DNTT) and its derivatives, which are widely employed in organic electronic devices 82,83, range from 75 meV to 188 meV 43, which is about 55 meV (22%) lower than our best reported reorganization energy in Lib-BDT spacer 0 (243 meV). On the other hand, the reorganization energy for naphthodithiophene diimide (NDTI), a recently synthesized derivative of widely studied n-type semiconductors NDI⁸¹, is around 286 meV⁸⁴, which is around 26% lower than our measured Lib-NDI spacer 1 (388 meV) and only 4% lower than Lib-PDI spacer 1 (301 meV).

Although our trends are non-monotonic, we find that reorganization energy tends to increase with increasing spacer size, degrading the charge mobility (c.f., Eqn. 6). To quantify this observation we measure the Pearson correlation coefficient ρ between spacer length and reorganization energy. The correlation coefficients are quite large and positive for the cationic systems: Lib-PTP ($\rho = 0.49$; p-value= 2.4×10^{-13}), Lib-QTP ($\rho = 0.56$; pvalue= 3.3×10^{-18}), and Lib-BDT ($\rho = 0.6$; p-value= 2.4×10^{-13}). They are weaker but still positive for the anionic systems: Lib-NDI ($\rho = 0.25$; p-value=3.4 × 10⁻⁴) and Lib-PDI ($\rho = 0.25$; pvalue= 4.7×10^{-4}). We propose that the weaker trends for Lib-NDI and Lib-PDI may stem from these two libraries being composed of more rigid aromatic cores compared to Lib-PTP, Lib-QTP, or Lib-BDT. Lastly, as a general trend for both hole and electron transport, we notice that independent of spacer size the more rigid aromatic cores composed of larger fused ring systems tend to result in smaller reorganization energies across the board, evidenced by Lib-BDT for holes and Lib-PDI for electrons.

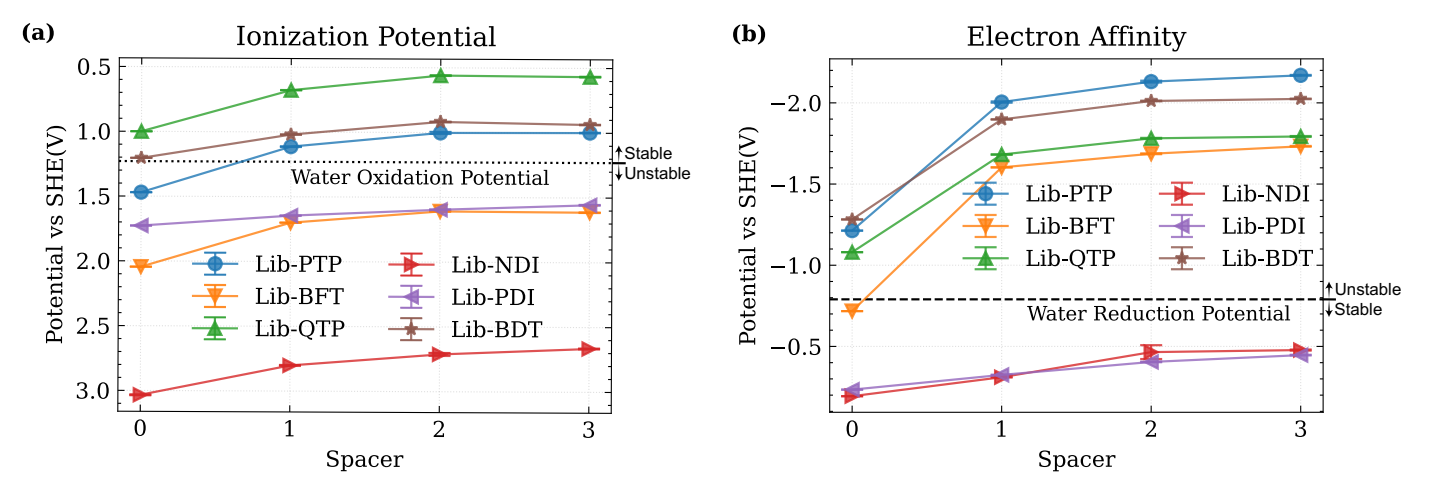


Fig. 3 The chemical stability of the cationic and anionic states of each oligopeptide in water. (a) Calculated ionization potentials relative to the water oxidation potential of +1.23 V (SHE). Molecules residing above the dashed horizontal line are predicted to support stable cationic states and serve as putative p-type semiconductors. (b) Calculated electron affinities relative to the water reduction potential of -0.83 V (SHE). Molecules residing below the dashed line are predicted to support stable anionic states and serve as putative n-type semiconductors.

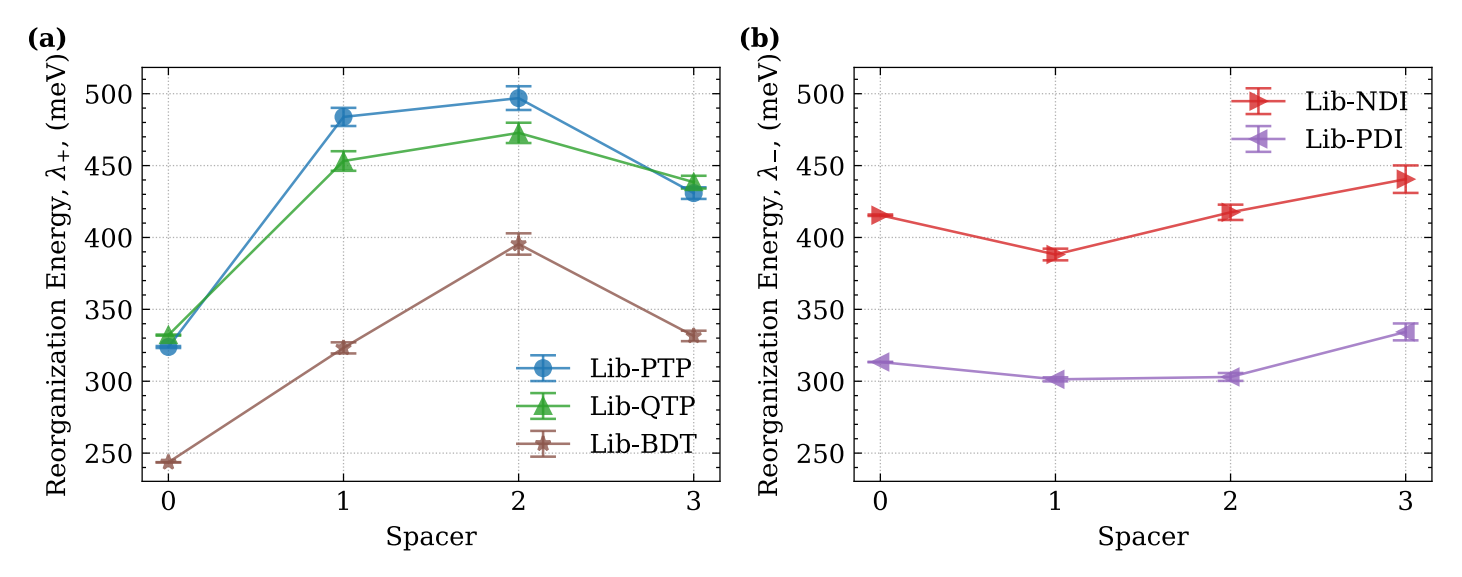


Fig. 4 Reorganization energies of the chemically stable aromatic core libraries. Smaller reorganization energies are associated with higher charge mobility. (a) Reorganization energies of the stable cationic molecules associated with hole transport in p-type semiconductors. (b) Reorganization energies of the stable anionic molecules associated with electron transport in n-type semiconductors. Error bars represent the standard error in the mean.

3.3 Transfer Integral

The transfer integral describes the strength of electronic coupling between neighboring molecules and is a strong function of the intermolecular distance and orientation. Large transfer integrals are desirable for good charge mobilities (c.f., Eqn. 6) and are associated with close structural alignment within the molecular pair leading to substantial overlap of electronic wavefunctions between the two molecules. Lower values for the transfer integral suggest weaker overlap of the individual molecular wavefunctions due to large intermolecular spacing and/or a transverse offset of the monomers within the dimer geometry. We present in Fig. 5 the transfer integrals calculated for holes and electrons in all chemically stable species. In the case of hole transport, we observe the values of our calculated transfer integrals to lie within a range of 18-82 meV (Fig. 5a). Although the transfer integral

heavily depends on the particular dimer geometries, previous literature has reported transfer integral values of $\sim\!\!96.7$ meV when the center of mass distance between pairs of DNTT is 4.374 Å 43 . This is the same order of magnitude that we observe for Lib-BDT spacer 0, which possesses transfer integral values of 82 meV at center of mass separations of $\sim\!\!4$ Å. In the case of electron transport, we find transfer integral values in the range 42–76 meV (Fig. 5b). In comparison, the transfer integral values for NDTI derivatives of 38-46 meV were reported at COM distances of 4.2 Å 84 , which is the same order of magnitude as our Lib-PDI spacer 0 that possess transfer integral values of 76 meV at COM separations of $\sim\!\!3.41$ Å.

While the trends in the transfer integrals with core chemistry and spacer length are more subtle than in the reorganization energy calculations, we notice that in hole transport Lib-QTP typi-

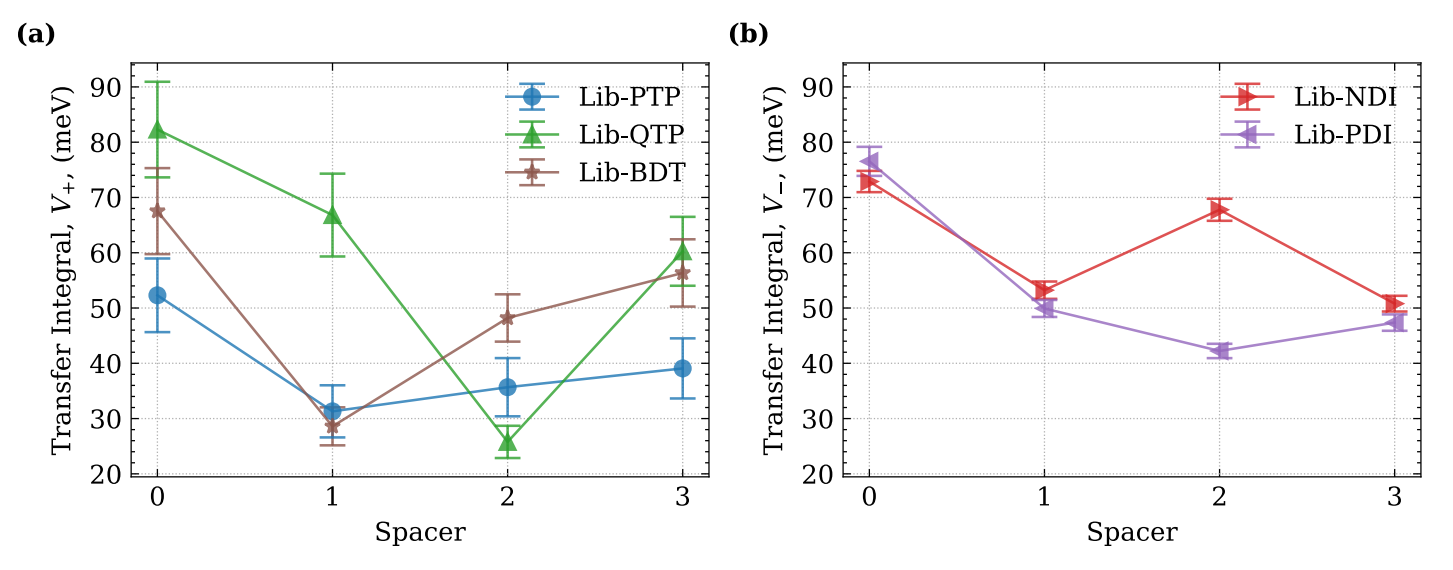


Fig. 5 Transfer integrals for the chemically stable aromatic core libraries. Larger transfer integrals are associated with higher charge mobility. (a) Transfer integrals between stable cationic molecules associated with hole transport in p-type semiconductors. (b) Transfer integrals between stable anionic molecules associated with electron transport in n-type semiconductors. Error bars represent the standard error in the mean.

cally performs better than Lib-PTP or Lib-BDT for smaller spacer lengths. For electron transport Lib-NDI and Lib-PDI perform similarly. Again, our trends are non-monotonic, but we observe relatively weak but negative correlations between transfer integral and spacer length: $\rho_{\text{Lib-PTP}} = -0.10$ (p-value=0.16), $\rho_{\text{Lib-QTP}} =$ -0.23 (p-value= 8.4×10^{-4}), $\rho_{\text{Lib-BDT}} = -0.04$ (p-value=0.6), $\rho_{\text{Lib-NDI}} = -0.05$ (p-value=0.48), $\rho_{\text{Lib-PDI}} = -0.24$ (p-value=5.8 × 10^{-4}). These trends indicate that increasing the spacer length tends to diminish the value of the transfer integral and signaling weaker intermolecular electronic coupling. Computing the Pearson correlation coefficient between the center-of-mass separation between pairs of molecules and the calculated transfer integral reveals uniformly negative, and in some cases quite strong, negative correlations: $\rho_{\text{Lib-PTP}} = -0.36$ (p-value=1.1 × 10^{-7}), $\rho_{\text{Lib-BDT}} = -0.31$ (p-value= 7.9×10^{-6}), $\rho_{\text{Lib-PDI}} = -0.082$ (p-value=0.25), $\rho_{\text{Lib-NDI}} = -0.12$ (p-value=0.086), $\rho_{\text{Lib-OTP}} =$ -0.18 (p-value=0.012) suggesting that higher transfer integral values correspond to π -conjugated peptide cores that are more tightly associated. These correlations also imply that, generally, smaller spacer lengths result in π -conjugated peptide nanoaggregates with closer intermolecular contacts.

3.4 Charge Mobility

Finally, we use Marcus theory (Eqns. 4, 5, and 6) to predict charge mobilities from our calculated reorganization energies and transfer integrals. We present in Fig. 6a the hole mobility and in Fig. 6b the electron mobility for all chemically stable species. We notice the hole mobility ranges between 0.003 and 0.224 $\rm cm^2/(Vs)$, while the electron mobility ranges between 0.024 and 0.143 $\rm cm^2/(Vs)$. In comparison, the hole mobility in DNTT and its derivatives reported in Ref. 43 range from 1.45 to 3.36 $\rm cm^2/(Vs)$, which is at least $\sim\!550\%$ higher than our best reported mobility of 0.224 $\rm cm^2/(Vs)$ in Lib-BDT spacer 0. On the other hand, the electron mobility of NDTI derivatives ranges from 0.24 to

0.39 cm²/(Vs) ⁸⁴, which is only ~71% higher than our highest electron mobility of 0.143 cm²/(Vs) in Lib-PDI spacer 0. We note that our predicted charge mobilities pertain to electron/hole transport along the π -cores in individual stacks of π -conjugated peptides and are commensurate with prior experimental reports of charge mobility within organic semiconductor nanowire structures ^{48,85,86}. We use these predictions as a consistent basis within which to compare the various π -conjugated peptides considered in this work, but appreciate that lower measured mobilities would be expected within films of these nanowires due to the presence of the insulating peptide side chains and possible attenuation effects due to the incorporation of these materials into a device ²¹.

Performing these charge mobility calculation serves as a comparative tool to help isolate the most promising π -conjugated peptides for optoelectronic applications. For hole mobility, we find that Lib-BDT with spacer 0 has the highest mobility at 0.224 cm²/(Vs) which is about 65% better than Lib-PTP spacer 0 and Lib-QTP spacer 0. This result is mainly due to the comparatively low reorganization energy for Lib-BDT which has an exponential dependence on the mobility, while the transfer integral only has a quadratic dependence based on Marcus theory (c.f., Eqn. 6). We also notice that Lib-QTP and Lib-PTP perform comparably to one another and similarly to Lib-BDT for spacer lengths of one and greater. For electron mobility, Lib-PDI with spacer 0 is the highest performing with an electron mobility of 0.143 cm²/(Vs) that is $\sim \!\! 320\%$ better than Lib-NDI spacer 2, once again primarily due to the low calculated value of the reorganization energy.

In general, we notice charge mobility to peak at zero spacer length and degrade, within error, for increasing spacer length for all calculated libraries, except for Lib-NDI which we find performs similarly poorly at all spacer lengths. We can once again quantify this trend by observing overall negative, and sometimes relatively large, correlations between charge mobility and spacer length: $\rho_{\text{Lib-PTP}} = -0.29$ (p-value= 3.9×10^{-5}), $\rho_{\text{Lib-QTP}} = -0.41$ (p-value= 2.6×10^{-9}), $\rho_{\text{Lib-NDI}} = -0.043$ (p-value=0.55), $\rho_{\text{Lib-PDI}} = -0.043$

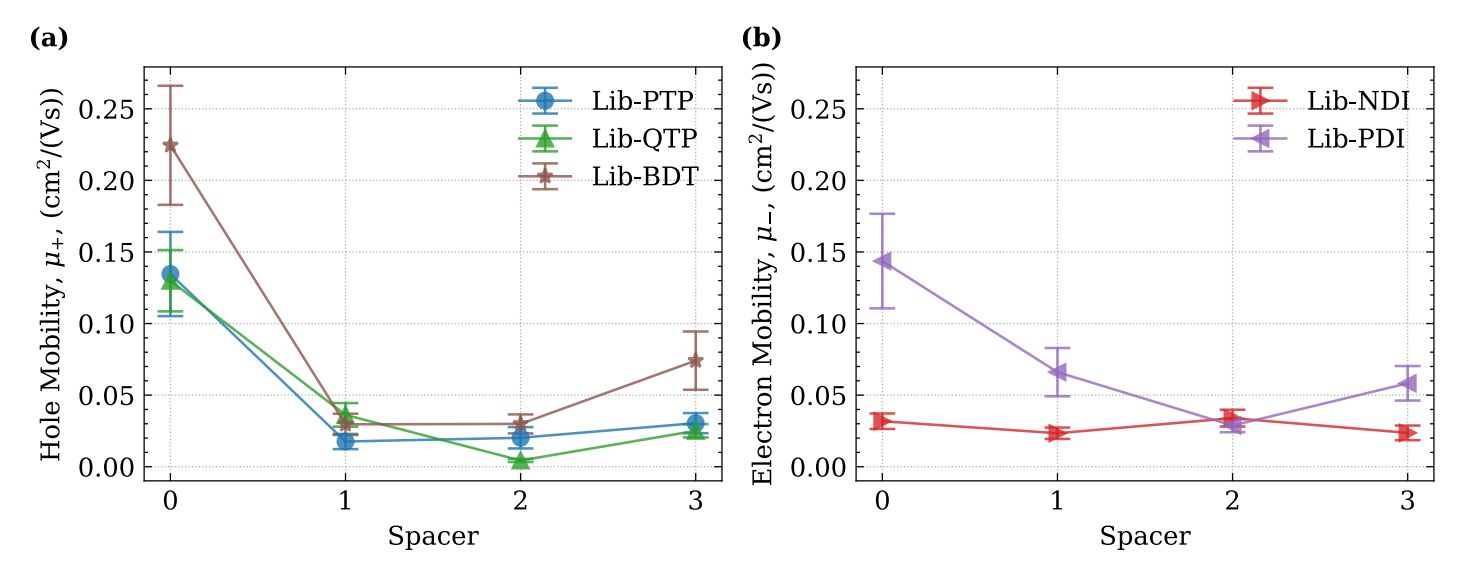


Fig. 6 Charge mobility predicted from the calculated reorganization energies and transfer integrals using Marcus theory. (a) Predicted hole mobilities in stable cationic molecules forming putative p-type semiconductors. (b) Predicted electron mobilities in stable anionic molecules forming putative n-type semiconductors. Error bars represent the standard error in the mean.

-0.23 (p-value=0.0012), $\rho_{\text{Lib-BDT}} = -0.27$ (p-value= 8.4×10^{-5}). Based on these results, we suggest Lib-BDT with zero spacer and Lib-PDI with zero spacer as the promising candidate p- and n-type organic semiconductors, respectively. Furthermore, we identify reorganization energy as the primary determinant of charge mobility in our case and that superior search efficiencies may be achieved when performing larger computational screenings by pre-screening molecules based on reorganization energy prior to performing transfer integral calculations.

4 Conclusions

In this study, we combine molecular dynamics simulations with first-principles electronic-structure calculations to predict the chemical stability and charge transport properties of a 24-molecule library of π -conjugated peptides containing one of six π -conjugated cores and with alkyl chain spacers of length $n \in \{0,1,2,3\}$ connecting the central aromatic cores to their flanking peptide wings (Fig. 1). For each library we perform electronic-structure calculations on a collection of dimer configurations harvested from molecular dynamics simulations of spontaneous self-assembly. Since these nanoaggregates lack a well-defined crystal structure, we are obliged to first perform molecular dynamics simulations of self-assembly to extract representative configurations to pass to the electronic structure calculations.

Chemical stability calculations serve as an initial filtration of our design space and are used to identify stable cationic and anionic candidates for putative hole and electron transport, respectively. Our stability calculations suggested that three of the candidate aromatic cores – phenyl-theophene-phenyl (Lib-PTP), quaterthiophene (Lib-QTP), and benzo-dithiophene (Lib-BDT) – have stable cationic states indicating that they are potential candidates for p-type semiconductors, whereas two of the candidate aromatic cores – naphthalene-diimide (Lib-NDI) and pyridine-diimide (Lib-PDI) – have stable anionic states indicating that they are potential candidates for n-type semiconductors. We then cal-

culate the reorganization energy and transfer integral for these molecules as inputs to Marcus theory charge mobility calculations. Our results identify benzo-dithiophene (Lib-BDT) with no alkyl spacer as possessing the highest predicted hole mobility of 0.224 cm 2 /(Vs), and pyridine-diimide (Lib-PDI) with no alkyl spacer as possessing the highest predicted electron mobility of 0.143 cm 2 /(Vs). In general, we find that charge mobility typically degrades with increasing spacer length, suggesting the absence of alkyl spacers as a more promising chemical motif for future study.

By combining molecular dynamics simulation and first-principles electronic-structure calculations we provide a detailed study of the chemical stability and charge mobility of π -conjugated peptide semiconductors. Although the calculated charge mobility values are lower than typical values that may be expected for crystalline semiconductors, π -conjugated peptide-based semiconductors possess advantages in terms of mechanical flexibility, solution processability, weight, aqueous stability, and biocompatibility, making them well-suited to charge transport and energy harvesting applications in biological and living systems. Our computational methodology is also expected to be generically extensible to screen other self-assembling and electronically active organic molecules.

Data Availability

Input files for the molecular dynamics simulations and electronic structure calculations along with MD trajectories, tabulated results of chemical stability, reorganization energy, transfer integral and charge mobility calculations, and post-processing scripts for the transfer integral calculation are provided via The Materials Data Facility (MDF) ^{87,88} at DOI:10.18126/ef9q-qzod ⁸⁹.

Author Contributions

KS performed the molecular simulations and YY performed the electronic structure calculations. KS and YY performed the data analysis. KS, YY, JDT, HEK, AS, and ALF designed the research.

KS, YY, AS and ALF wrote the manuscript. JDT, HEK, AS, and ALF edited the manuscript.

Conflicts of interest

ALF is a co-founder and consultant of Evozyne, Inc. and a co-author of US Provisional Patents 62/853,919 and 62/900,420 and International Patent Applications PCT/US2020/035206 and PCT/US20/50466.

Acknowledgements

This work is supported by the National Science Foundation under Grant Nos. DMR-1841807 and DMR-1728947. KS is supported by the National Science Foundation Graduate Research Fellowship under Grant No. DGE-1746045. This work was completed in part with resources provided by the University of Chicago Research Computing Center. We gratefully acknowledge computing time on the University of Chicago high-performance GPU-based cyberinfrastructure supported by the National Science Foundation under Grant No. DMR-1828629. We thank Sayak Subhra Panda and Taein Lee for helpful discussions.

Notes and references

- 1 Conjugated Polymers for Biological and Biomedical Applications, ed. B. L. Liu, Wiley-VCH Verlag GmbH & Co. KGaA, Weinheim, Germany, 2018.
- 2 R. Mondal, S. Ko and Z. Bao, *Journal of Materials Chemistry*, 2010, **20**, 10568.
- 3 L. Lu, T. Zheng, Q. Wu, A. M. Schneider, D. Zhao and L. Yu, *Chemical Reviews*, 2015, **115**, 12666–12731.
- 4 S. S. Panda, H. E. Katz and J. D. Tovar, *Chemical Society Reviews*, 2018, **47**, 3640–3658.
- 5 H. A. M. Ardoña and J. D. Tovar, *Bioconjugate Chemistry*, 2015, **26**, 2290–2302.
- 6 M. A. Khalily, G. Bakan, B. Kucukoz, A. E. Topal, A. Karatay, H. G. Yaglioglu, A. Dana and M. O. Guler, ACS Nano, 2017, 11, 6881–6892.
- 7 R. S. Moghaddam, E. R. Draper, C. Wilson, H. Heidari and D. J. Adams, *RSC Advances*, 2018, **8**, 34121–34125.
- 8 G. L. Eakins, R. Pandey, J. P. Wojciechowski, H. Y. Zheng, J. E. Webb, C. Valéry, P. Thordarson, N. O. Plank, J. A. Gerrard and J. M. Hodgkiss, *Advanced Functional Materials*, 2015, **25**, 5640–5649.
- 9 M. Pandeeswar, H. Khare, S. Ramakumar and T. Govindaraju, *Chemical Communications*, 2015, **51**, 8315–8318.
- 10 J. López-Andarias, M. J. Rodriguez, C. Atienza, J. L. López, T. Mikie, S. Casado, S. Seki, J. L. Carrascosa and N. Martín, Journal of the American Chemical Society, 2015, 137, 893– 897.
- 11 J. D. Tovar, Accounts of Chemical Research, 2013, **46**, 1527–1537.
- 12 M. Amit, S. Yuran, E. Gazit, M. Reches and N. Ashkenasy, *Advanced Materials*, 2018, **30**, 1707083.
- 13 D. M. Raymond and B. L. Nilsson, *Chemical Society Reviews*, 2018, **47**, 3659–3720.

- 14 R. V. Ulijn and A. M. Smith, *Chemical Society Reviews*, 2008, 37, 664–675.
- 15 A. B. Marciel, M. Tanyeri, B. D. Wall, J. D. Tovar, C. M. Schroeder and W. L. Wilson, *Advanced Materials*, 2013, **25**, 6398–6404.
- 16 R. A. Mansbach and A. L. Ferguson, *Organic & Biomolecular Chemistry*, 2017, **15**, 5484–5502.
- 17 A. P. Schenning and E. Meijer, *Chemical Communications*, 2005, 3245–3258.
- 18 M. Mba, A. Moretto, L. Armelao, M. Crisma, C. Toniolo and M. Maggini, *Chemistry–A European Journal*, 2011, 17, 2044– 2047.
- 19 J. K. Gallaher, E. J. Aitken, R. A. Keyzers and J. M. Hodgkiss, *Chemical Communications*, 2012, **48**, 7961–7963.
- 20 E. R. Jira, K. Shmilovich, T. S. Kale, A. Ferguson, J. D. Tovar and C. M. Schroeder, *ACS Applied Materials & Interfaces*, 2020, **12**, 20722–20732.
- 21 T. Lee, S. S. Panda, J. D. Tovar and H. E. Katz, *ACS Nano*, 2020, **14**, 1846–1855.
- 22 A. Facchetti, Chemistry of Materials, 2011, 23, 733-758.
- 23 L. Bian, E. Zhu, J. Tang, W. Tang and F. Zhang, *Progress in Polymer Science*, 2012, **37**, 1292–1331.
- 24 B. D. Wall, A. E. Zacca, A. M. Sanders, W. L. Wilson, A. L. Ferguson and J. D. Tovar, *Langmuir*, 2014, **30**, 5946–5956.
- 25 P. M. Beaujuge and J. R. Reynolds, *Chemical Reviews*, 2010, **110**, 268–320.
- 26 H. A. M. Ardoña and J. D. Tovar, Chemical Science, 2015, 6, 1474–1484.
- 27 B. A. Thurston, J. D. Tovar and A. L. Ferguson, *Molecular Simulation*, 2016, **42**, 955–975.
- 28 L. R. Valverde, B. A. Thurston, A. L. Ferguson and W. L. Wilson, *Langmuir*, 2018, **34**, 7346–7354.
- 29 S. S. Panda, K. Shmilovich, N. S. Herringer, N. Marin, A. L. Ferguson and J. D. Tovar, *Langmuir*, 2021, 37, 8594–8606.
- 30 S. S. Panda, K. Shmilovich, A. L. Ferguson and J. D. Tovar, *Langmuir*, 2019, **35**, 14060–14073.
- 31 S. S. Panda, K. Shmilovich, A. L. Ferguson and J. D. Tovar, *Langmuir*, 2020, **36**, 6782–6792.
- 32 Y. Liu, D. Zhang, B. Ren, X. Gong, L. Xu, Z.-Q. Feng, Y. Chang, Y. He and J. Zheng, *Journal of Materials Chemistry B*, 2020, **8**, 3814–3828.
- 33 Y. Liu, D. Zhang, Y. Tang, Y. Zhang, X. Gong, S. Xie and J. Zheng, *Chemical Engineering Journal*, 2021, **420**, 129872.
- 34 B. A. Thurston, E. P. Shapera, J. D. Tovar, A. Schleife and A. L. Ferguson, *Langmuir*, 2019, **35**, 15221–15231.
- 35 R. A. Mansbach and A. L. Ferguson, *The Journal of Physical Chemistry B*, 2017, **121**, 1684–1706.
- 36 K. Shmilovich, R. A. Mansbach, H. Sidky, O. E. Dunne, S. S. Panda, J. D. Tovar and A. L. Ferguson, *The Journal of Physical Chemistry B*, 2020, **124**, 3873–3891.
- 37 B. A. Thurston and A. L. Ferguson, *Molecular Simulation*, 2018, 44, 930–945.
- 38 R. A. Mansbach and A. L. Ferguson, *The Journal of Physical Chemistry B*, 2018, **122**, 10219–10236.

- 39 K. Shmilovich, S. Panda, A. Stouffer, J. Tovar and A. Ferguson, ChemRxiv preprint: 10.33774/chemrxiv-2021-l42ch, 2021.
- 40 H. Oberhofer, K. Reuter and J. Blumberger, Chemical Reviews, 2017, 117, 10319-10357.
- 41 I. Yavuz, B. N. Martin, J. Park and K. N. Houk, Journal of the American Chemical Society, 2015, 137, 2856-2866.
- 42 G. Gryn'ova, K.-H. Lin and C. Corminboeuf, Journal of the American Chemical Society, 2018, 140, 16370-16386.
- 43 A. N. Sokolov, S. Atahan-Evrenk, R. Mondal, H. B. Akkerman, R. S. Sánchez-Carrera, S. Granados-Focil, J. Schrier, S. C. Mannsfeld, A. P. Zoombelt, Z. Bao and A. Aspuru-Guzik, Nature Communications, 2011, 2, 437.
- 44 R. A. Marcus, Annual Review of Physical Chemistry, 1964, 15, 155-196.
- 45 Y. A. Berlin, G. R. Hutchison, P. Rempala, M. A. Ratner and J. Michl, The Journal of Physical Chemistry A, 2003, 107, 3970-3980.
- 46 A. M. Sanders, T. J. Dawidczyk, H. E. Katz and J. D. Tovar, ACS Macro Letters, 2012, 1, 1326-1329.
- 47 A. J. Petty, Q. Ai, J. C. Sorli, H. F. Haneef, G. E. Purdum, A. Boehm, D. B. Granger, K. Gu, C. P. L. Rubinger, S. R. Parkin, K. R. Graham, O. D. Jurchescu, Y.-L. Loo, C. Risko and J. E. Anthony, Chemical Science, 2019, 10, 10543–10549.
- 48 Z. Hu, Z. Lin, J. Su, J. Zhang, Y. Hao, J. Chang and J. Wu, ACS Applied Electronic Materials, 2019, 1, 2030–2036.
- 49 B. J. Jung, K. Lee, J. Sun, A. G. Andreou and H. E. Katz, Advanced Functional Materials, 2010, 20, 2930-2944.
- 50 M. Funahashi and J.-I. Hanna, Molecular Crystals and Liquid Crystals, 2005, 436, 225-1179.
- 51 A. Facchetti, M.-H. Yoon, C. L. Stern, H. E. Katz and T. J. Marks, Angewandte Chemie, 2003, 115, 4030-4033.
- 52 K. Besar, H. A. M. Ardoña, J. D. Tovar and H. E. Katz, ACS Nano, 2015, 9, 12401-12409.
- 53 W. Humphrey, A. Dalke and K. Schulten, Journal of Molecular Graphics, 1996, 14, 33-38.
- 54 K. Momma and F. Izumi, Journal of Applied Crystallography, 2011, 44, 1272-1276.
- 55 M. J. Abraham, T. Murtola, R. Schulz, S. Páll, J. C. Smith, B. Hess and E. Lindahl, SoftwareX, 2015, 1, 19-25.
- 56 C. A. Reynolds, J. W. Essex and W. G. Richards, Journal of the American Chemical Society, 1992, 114, 9075–9079.
- 57 W. D. Cornell, P. Cieplak, C. I. Bayly and P. A. Kollman, Journal of the American Chemical Society, 2002, 115, 9620–9631.
- 58 M. J. Frisch, G. W. Trucks, H. B. Schlegel, G. E. Scuseria, M. A. Robb, J. R. Cheeseman, G. Scalmani, V. Barone, G. A. Petersson, H. Nakatsuji, X. Li, M. Caricato, A. V. Marenich, J. Bloino, B. G. Janesko, R. Gomperts, B. Mennucci, H. P. Hratchian, J. V. Ortiz, A. F. Izmaylov, J. L. Sonnenberg, D. Williams-Young, F. Ding, F. Lipparini, F. Egidi, J. Goings, B. Peng, A. Petrone, T. Henderson, D. Ranasinghe, V. G. Zakrzewski, J. Gao, N. Rega, G. Zheng, W. Liang, M. Hada, M. Ehara, K. Toyota, R. Fukuda, J. Hasegawa, M. Ishida, T. Nakajima, Y. Honda, O. Kitao, H. Nakai, T. Vreven, K. Throssell, J. A. Montgomery, Jr., J. E. Peralta, F. Ogliaro, M. J. Bearpark, J. J.

- Heyd, E. N. Brothers, K. N. Kudin, V. N. Staroverov, T. A. Keith, R. Kobayashi, J. Normand, K. Raghavachari, A. P. Rendell, J. C. Burant, S. S. Iyengar, J. Tomasi, M. Cossi, J. M. Millam, M. Klene, C. Adamo, R. Cammi, J. W. Ochterski, R. L. Martin, K. Morokuma, O. Farkas, J. B. Foresman and D. J. Fox, Gaussian 16 Revision C.01, 2016.
- 59 A. W. S. Da Silva and W. F. Vranken, BMC Research Notes, 2012, 5, 1-8.
- 60 D. Case, D. Cerutti, T. Cheatham, T. Darden, R. Duke, T. Giese, H. Gohlke, A. Götz, D. Greene, N. Homeyer, S. Izadi, A. Kovalenko, T.-S. Lee, S. LeGrand, P. Li, C. Lin, J. Liu, T. Luchko, R. Luo and P. Kollman, Amber 2017, University of California, San Francisco, 2017.
- 61 K. Lindorff-Larsen, S. Piana, K. Palmo, P. Maragakis, J. L. Klepeis, R. O. Dror and D. E. Shaw, Proteins: Structure, Function, and Bioinformatics, 2010, 78, 1950-1958.
- 62 R. W. Hockney and J. W. Eastwood, Computer Simulation Using Particles, CRC Press, 1988.
- 63 B. Hess, H. Bekker, H. J. Berendsen and J. G. Fraaije, Journal of Computational Chemistry, 1997, 18, 1463-1472.
- 64 U. Essman, L. Perera, M. Berkowitz, T. Darden, H. Lee and L. Pedersen, Journal of Chemical Physics, 1995, 103, 8577-8592.
- 65 P. Mark and L. Nilsson, The Journal of Physical Chemistry A, 2001, **105**, 9954–9960.
- 66 G. Bussi, D. Donadio and M. Parrinello, Journal of Chemical Physics, 2007, 126, 014101.
- 67 M. Parrinello and A. Rahman, Journal of Applied Physics, 1981, **52**, 7182–7190.
- 68 H. A. M. Ardoña, PhD thesis, Johns Hopkins University, 2017.
- 69 H. A. M. Ardoña, E. R. Draper, F. Citossi, M. Wallace, L. C. Serpell, D. J. Adams and J. D. Tovar, Journal of the American Chemical Society, 2017, 139, 8685-8692.
- 70 K. Molčanov, V. Milašinović and B. Kojić-Prodić, Crystal Growth & Design, 2019, 19, 5967-5980.
- 71 J. Tomasi, B. Mennucci and R. Cammi, Chemical Reviews, 2005, **105**, 2999–3094.
- 72 C. Lee, W. Yang and R. G. Parr, Physical Review B, 1988, 37, 785-789.
- 73 A. D. Becke, Journal of Chemical Physics, 1993, 98, 5648-
- 74 D. de Leeuw, M. Simenon, A. Brown and R. Einerhand, Synthetic Metals, 1997, 87, 53-59.
- 75 R. Di Pietro, D. Fazzi, T. B. Kehoe and H. Sirringhaus, Journal of the American Chemical Society, 2012, **134**, 14877–14889.
- 76 S. G. Bratsch, Journal of Physical and Chemical Reference Data, 1989, 18, 1-21.
- 77 O. López-Estrada, H. G. Laguna, C. Barrueta-Flores and C. Amador-Bedolla, ACS Omega, 2018, 3, 2130–2140.
- 78 J.-L. Brédas, D. Beljonne, V. Coropceanu and J. Cornil, Chemical Reviews, 2004, 104, 4971-5004.
- 79 S. Chaudhuri, S. Hedström, D. D. Méndez-Hernández, H. P. Hendrickson, K. A. Jung, J. Ho and V. S. Batista, Journal of Chemical Theory and Computation, 2017, 13, 6000-6009.

- 80 B. Baumeier, J. Kirkpatrick and D. Andrienko, Physical Chemistry Chemical Physics, 2010, 12, 11103.
- 81 J. T. E. Quinn, J. Zhu, X. Li, J. Wang and Y. Li, Journal of Materials Chemistry C, 2017, 5, 8654-8681.
- 82 U. Zschieschang, T. Yamamoto, K. Takimiya, H. Kuwabara, M. Ikeda, T. Sekitani, T. Someya and H. Klauk, Advanced Materials, 2011, 23, 654-658.
- 83 T. Sekitani, T. Yokota, K. Kuribara, M. Kaltenbrunner, T. Fukushima, Y. Inoue, M. Sekino, T. Isoyama, Y. Abe, H. Onodera and T. Someya, Nature Communications, 2016, 7, 11425.
- 84 G. Ricci, S. Canola, Y. Dai, D. Fazzi and F. Negri, Molecules, 2021, 26, 4119.
- 85 L. R. Fleet, J. Stott, B. Villis, S. Din, M. Serri, G. Aeppli,

- S. Heutz and A. Nathan, ACS Applied Materials & Interfaces, 2017, 9, 20686-20695.
- 86 Y. Zhou, T. Lei, L. Wang, J. Pei, Y. Cao and J. Wang, Advanced Materials, 2010, 22, 1484-1487.
- 87 B. Blaiszik, K. Chard, J. Pruyne, R. Ananthakrishnan, S. Tuecke and I. Foster, JOM: The Journal of The Minerals, Metals & Materials Society (TMS), 2016, 68, 2045-2052.
- 88 B. Blaiszik, L. Ward, M. Schwarting, J. Gaff, R. Chard, D. Pike, K. Chard and I. Foster, MRS Communications, 2019, 9, 1125-1133.
- 89 K. Shmilovich, Y. Yao, J. D. Tovar, H. E. Katz, A. Schleife and A. L. Ferguson, Supplemental data for "Computational discovery of high charge mobility self-assembling π -conjugated peptides", 2022, https://doi.org/10.18126/ef9q-qzod.

SUPPORTING INFORMATION:

Computational discovery of high charge mobility self-assembling π -conjugated peptides

Kirill Shmilovich, $^{\dagger,\#}$ Yifan Yao, $^{\ddagger,\#}$ John D. Tovar, ¶,§ Howard E. Katz, § André Schleife, $^{*,\parallel}$ and Andrew L. Ferguson $^{*,\perp}$

†Pritzker School of Molecular Engineering, University of Chicago, Chicago, Illinois 60637, USA.

- ‡ Department of Materials Science and Engineering, University of Illinois,
 Urbana-Champaign, Urbana, Illinois 61801, USA.
- ¶ Department of Chemistry, Johns Hopkins University, 3400 North Charles Street,
 Baltimore, Maryland 21218, USA.
- § Department of Materials Science and Engineering, Johns Hopkins University, 3400 North

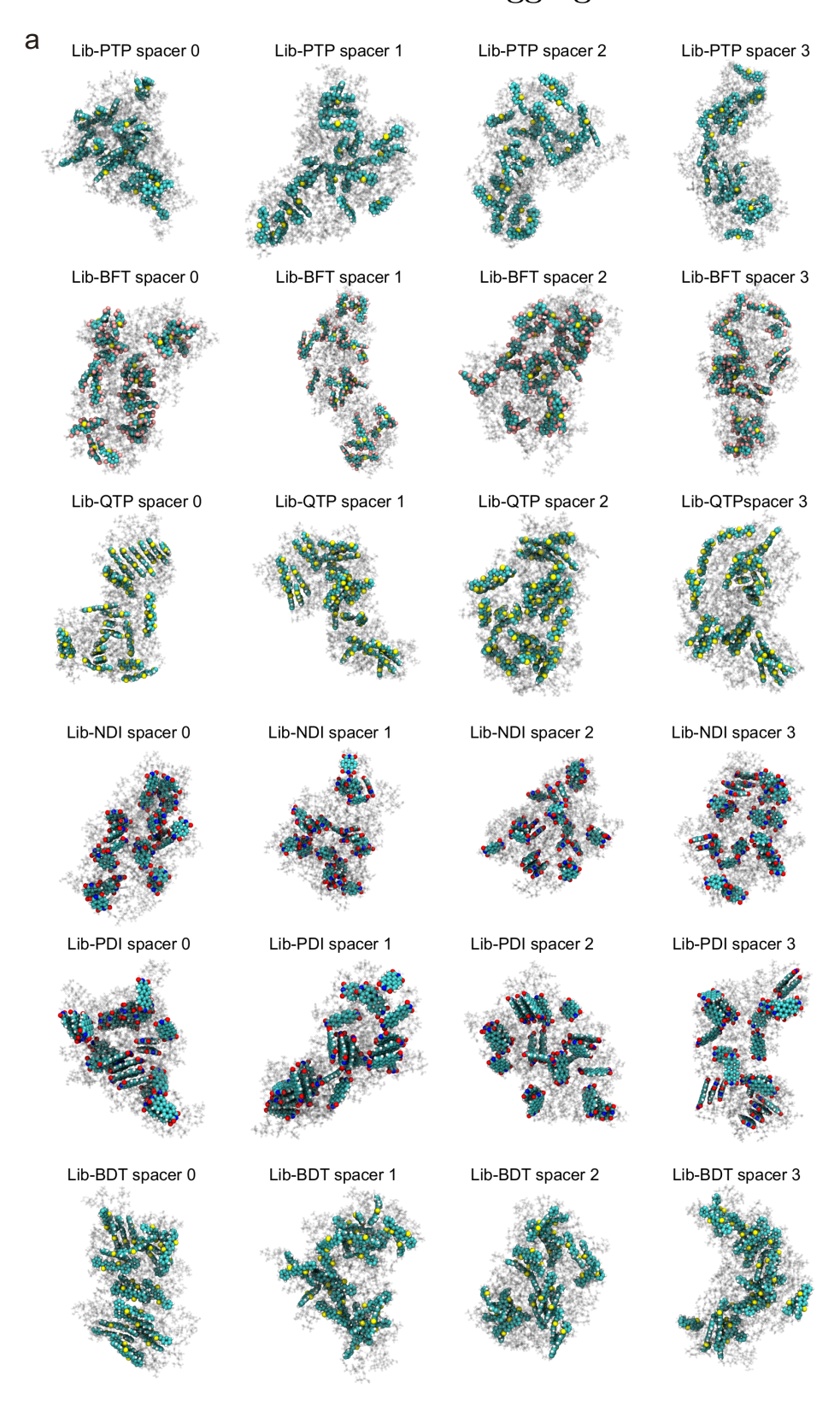
 Charles Street, Baltimore, Maryland 21218, USA.
 - || Department of Materials Science and Engineering, University of Illinois at Urbana-Champaign, Urbana, Illinois 61801, USA.
 - ⊥ Pritzker School of Molecular Engineering, University of Chicago, Chicago, Illinois 60637, USA.

 $\#Equal\ contribution$

E-mail: schleife@illinois.edu; andrewferguson@uchicago.edu

Supporting Methods

MD simulation of self-assembled nanoaggregates



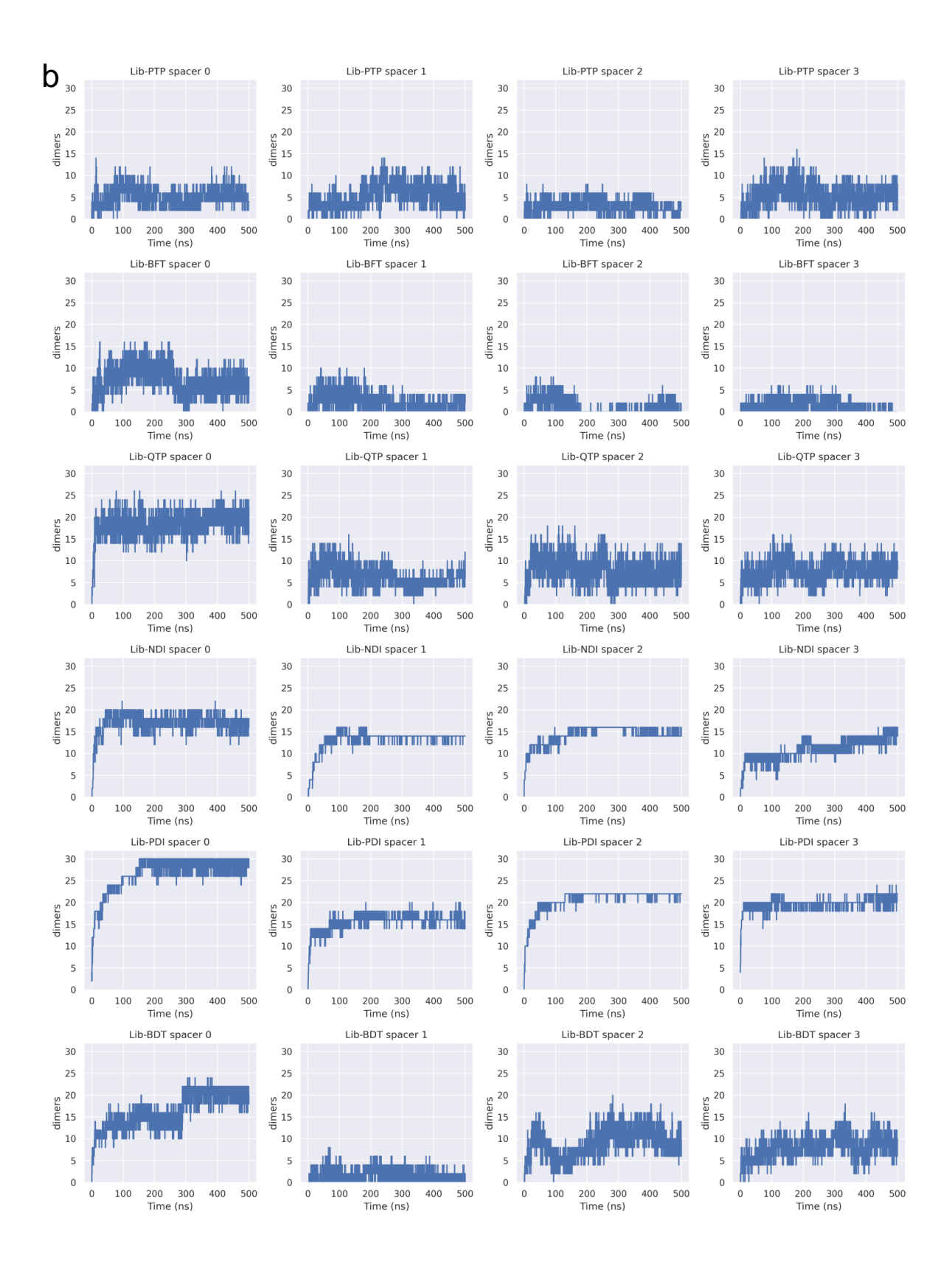


Figure S1: (a) Visualizations of the terminal simulation snapshots for each π -conjugated peptide system studied in this work. The π -cores are rendered as space-filling spheres while the spacer and peptide wings are faded gray and the water solvent is removed for clarity. (b) Number of dimers observed over the course of the MD simulation for each candidate molecule. A pair of molecules i and j within a simulation frame is defined to be a dimer if the COM distance between their aromatic cores satisfies $d_{i,j} \leq 0.5$ nm. The number of dimers within each system stabilizes after 375 ns indicating completion of the self-assembly process and the assembly of morphologically stable nanoaggregates. Dimers are harvested over the terminal 125 ns to be passed to the DFT calculations.

Transfer integral calculation scheme

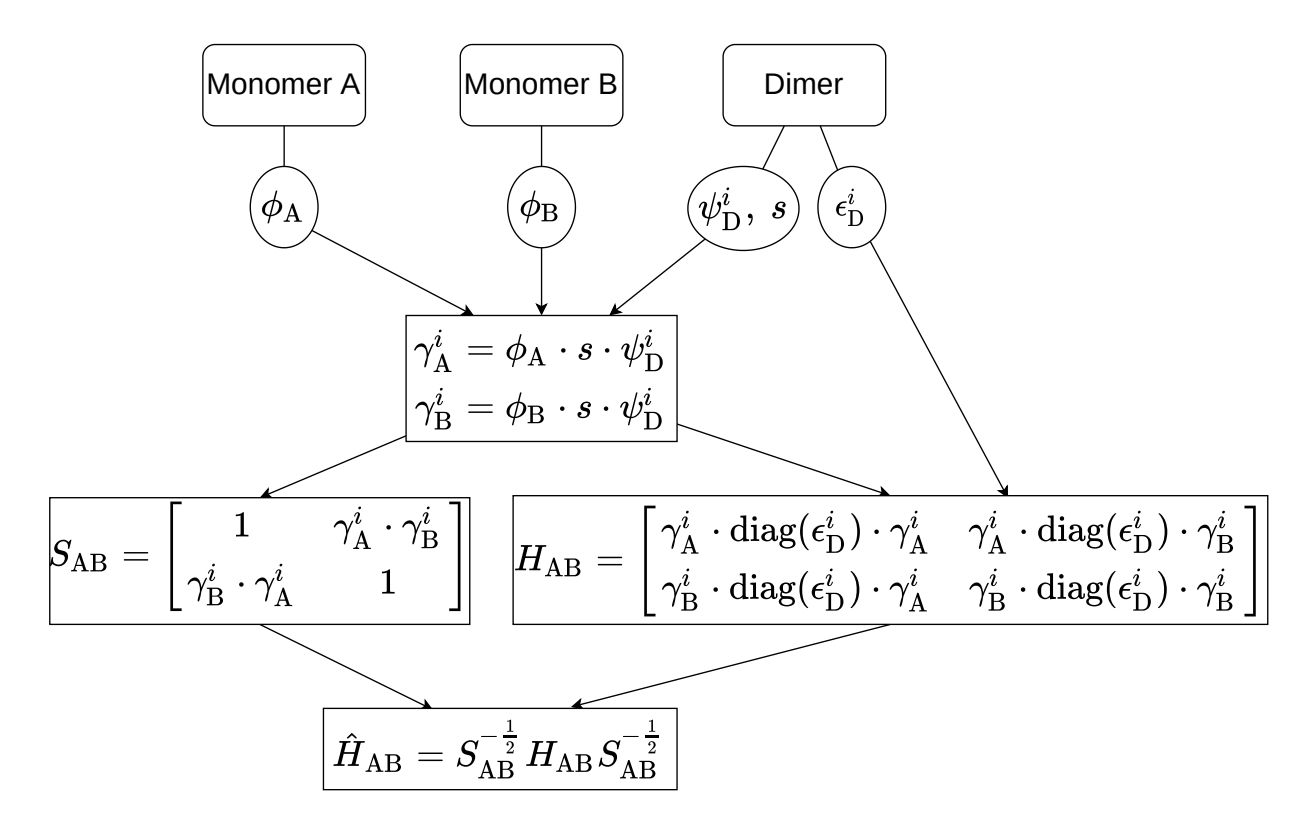


Figure S2: Diagram of the procedure for calculating the transfer integral V_{\pm} . First, we project the monomer frontier orbital $\phi_{\rm A}$ and $\phi_{\rm B}$ onto the dimer orbitals $\psi_{\rm D}^i$ with dimer orbital energies $\epsilon_{\rm D}^i$ to form γ_A^i and γ_B^i . s is the overlap matrix of the atomic orbital basis used in Gaussian 16. S is the overlap matrix of the monomer orbitals. The overlap and Hamiltonian matrices are subjected to Löwdin orthornomalization. V_{\pm} is given by the off-diagonal term of $\hat{H}_{\rm AB}$.

Transfer integral in isolated dimer and tetramer-embedded dimer

To validate the dimer approximation, we extend our transfer integral calculation from an isolated PTP dimer to a PTP dimer embedded within a tetramer stack. The only modification of this scheme is that γ is the tetramer orbitals instead of dimer orbitals, and the local monomer frontier orbitals are projected onto tetramer orbitals. An example of the geometry is depicted in Fig. S3. To reduce the computational cost for tetramers, we adopt a cheaper basis set, 6-31G(d). The small difference in the hole mobilities calculated based on the transfer integral computed in an isolated dimer and in a dimer embedded in tetramer presented in Table S1 confirm the validity of the dimer approximation.

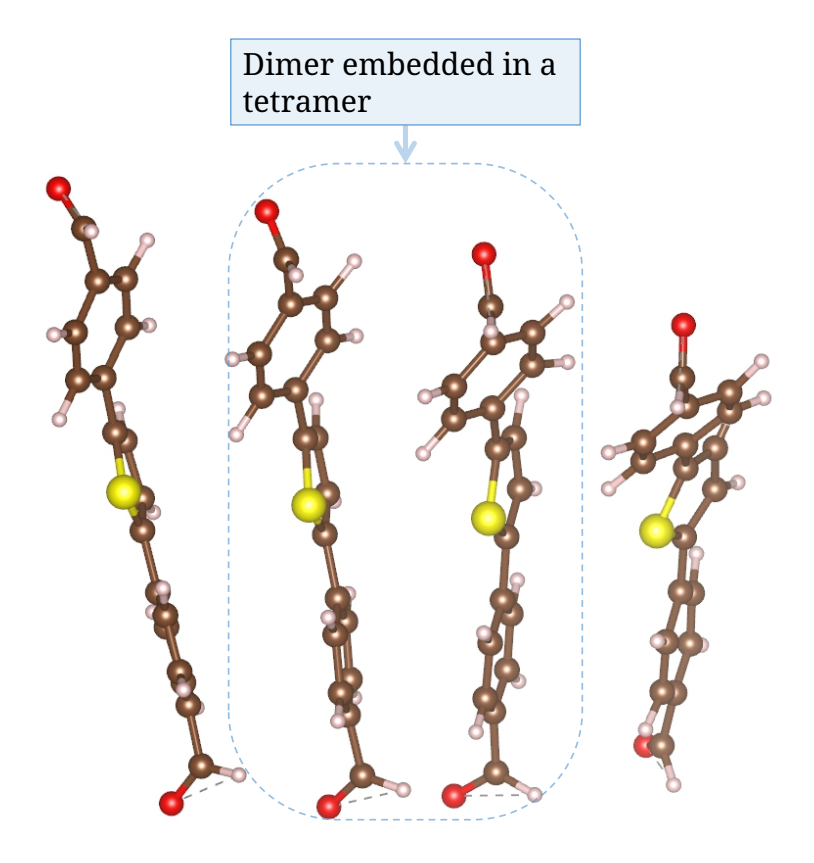


Figure S3: Dimer embedded in tetramer

Table S1: Charge mobility of isolated dimer and dimer embedded in tetramer

	hole mobility $(10^{-2} \times \text{cm}^2/(\text{Vs}))$		
	isolated dimer	dimer embeded in tetramer	Relative Difference(%)
Lib-PTP spacer 0	2.3365	2.3087	-1.19
Lib-PTP spacer 0	-2.9843	-2.9649	-0.65
Lib-PTP spacer 0	2.9158	2.9087	-0.24
Lib-PTP spacer 1	0.8513	0.8559	0.54
Lib-PTP spacer 1	-2.4482	-2.1728	-11.25
Lib-PTP spacer 1	0.0353	0.0355	0.46
Lib-PTP spacer 2	0.7425	0.7397	-0.37
Lib-PTP spacer 2	0.1942	0.1893	-2.50
Lib-PTP spacer 2	-0.4039	-0.4058	0.46
Lib-PTP spacer 3	3.3444	3.3276	-0.50
Lib-PTP spacer 3	-6.1775	-6.1731	-0.07
Lib-PTP spacer 3	-3.3790	-3.3773	-0.05

Supporting justification for $\Delta G_{\pm} = 0$ approximation

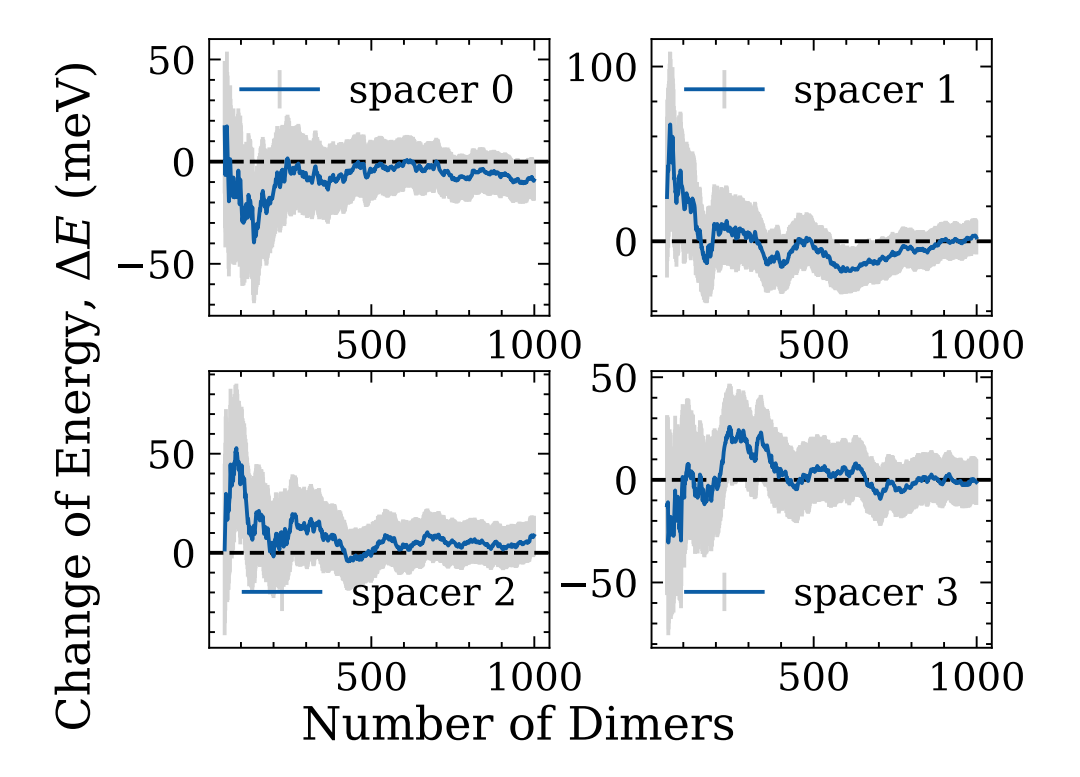


Figure S4: Difference of total energy $\Delta E = E_0(\mathrm{A}^0) - E_0(\mathrm{B}^0)$ between monomer A and monomer B within dimer pairs of the Lib-PTP system as a function of the size of the dimer ensemble. The shaded grey area denotes the standard error of the mean. As expected by the chemical indistinguishability of the two arbitrarily labeled A and B monomers constituting the dimer, $\Delta E \to 0$ for sufficiently large dimer ensembles.